

## **The collision/reaction cell and its application in inductively coupled plasma mass spectrometry for the determination of radioisotopes: A literature review**

**Mohamed A. Amr<sup>\*1&2</sup>**

<sup>1</sup>Central Laboratories unit, Office of Research, Qatar University, Doha, 2713, Qatar

<sup>2</sup>Nuclear Physics Department, NRC, Atomic Energy Authority, Cairo, Egypt

---

### **ABSTRACT**

*Inductively coupled plasma mass spectrometry (ICP-MS) is reviewed as an alternative nuclear analytical technique for the determination of radioisotopes. The latest development and utilization of collision and reaction cells in ICP-MS is presented. These cells are used to promote reactive and non-reactive collisions with resultant benefits in interference reduction, isobar separation, and thermalization/focusing of ions in ICP-MS. Novel ion-molecule chemistry schemes, using a variety of reaction gas reagents selected on the basis of thermodynamic and kinetic principles and data, are now designed and empirically evaluated with relative ease, and a significant body of ICP-MS applications now exists in the literature. Results for separations of isobaric overlaps via cation reactions with NO, N<sub>2</sub>O, O<sub>2</sub>, CO<sub>2</sub>, C<sub>2</sub>H<sub>2</sub>, and CH<sub>3</sub>F in an inductively coupled plasma collision/reaction cell mass spectrometer (ICP-CRC-MS) are reviewed.*

**Key words:** ICP-MS, Radioisotopes, Collision/Reaction Cell, Ion-molecule reaction

---

### **1. Inductively Coupled Plasma Mass Spectrometry (ICP-MS)**

The inductively coupled plasma (ICP) ion source is a special type of plasma that derives its sustaining power by induction from a high-frequency magnetic field [1]. Argon gas initially flows through a 25-mm quartz tube, and after emerging at the tip, it is surrounded by an induction coil. An AC current flows through this coil at a frequency of approximately 27 or 40 MHz at a power level of approximately 1.6 kW. The argon gas stream (the support gas) that enters the coil is initially seeded with free electrons from a Tesla coil. These seed electrons quickly interact with the magnetic field of the coil and gain sufficient energy to ionize the argon atoms through collisional excitation. The cations and electrons that are generated from the initial Tesla spark are accelerated by the magnetic field into a circular flow that is perpendicular to the stream that emerges from the tip of the torch. Reversing the direction of the current in the induction coil reverses the direction of the magnetic field that is applied to the mixture of atoms, ions and electrons. The fast-moving cations and electrons, which are known as an eddy current, collide with more argon atoms to produce further ionization and intense thermal energy. Flame-shaped plasma is formed near the top of the torch. The temperatures in the plasma range from 6000 to 10000 K. The high temperatures produced by the plasma generally require a second stream of gas, usually argon, to provide a vortex flow of argon to cool the inner quartz walls of the torch. This flow also serves to center and stabilize the plasma.

Liquid samples are usually introduced into the plasma in a stream of argon in the form of an aerosol obtained by the pneumatic nebulization of the solution. The argon stream punctures the plasma, which forms a central channel where the atomization and ionization occur. At frequencies of 27 or 40 MHz, a phenomenon known as the skin effect occurs; this effect gives the ICP plasma a toroidal shape. This plasma shaping lengthens the resident time (approximately 2 msec) of the sample in the high-temperature interior zone of the plasma and increases the detection limits of many elements [2]. A long, well-defined tail emerges from the high temperature plasma on the tip of the torch. This tail is the spectroscopic source, which contains all of the analyte atoms and ions that have been excited by the heat of the plasma. A portion of the ionized gas from the tail flame of the ICP is introduced into the vacuum system of the mass spectrometer. The plasma tail flame flows around the tip of a water-cooled cone, which is called

the sampler. The gas from the ICP is extracted through a small aperture (0.4-0.8 mm) that is drilled into the cone and into the first (expansion) stage that operates at a pressure of approximately 1 torr. The central orifice of the conical skimmer is located behind the sampler at an appropriate position for transmitting as much of the sampled beam as possible into a second vacuum chamber. The pressure in the second chamber is sufficiently low (approximately  $5 \times 10^{-4}$  torr) and the mean free path is sufficiently long for the ion lenses to collect, focus and transmit the ions to the mass analyzer. The ions delivered from the ICP source are accordingly focused by the electrostatic lenses. After the ions enter the mass spectrometer, they are separated by their mass-to-charge ratio.

A quadrupole mass filter is the most commonly used filter in mass spectrometers. This filter consists of four rods (approximately 1 cm in diameter and 15-20 cm long) that are arranged in perpendicular pairs. Alternating AC and DC voltages are applied to opposite pairs of the rods, which allow the ions with a single mass-to-charge ratio ( $m/z$ ) to pass through the rods to the detector at a specific point in time. The settings are altered for each specific  $m/z$ , and they are switched at a very rapid rate. Consequently, the quadrupole mass filter can separate up to 2400 amu (atomic mass units) per second [3].

Quadrupole mass filters used in ICP-MS have resolutions of almost one atomic mass unit [2]. This resolution is sufficient for most routine applications. However, there are some situations in which this resolution is not sufficient for separating overlapping polyatomic or isobaric interferences from the elemental isotope of interest. Thus, the use of high resolution (HR) or sector field (SF) mass spectrometers has become more common in ICP-MS; these instruments allow the user to eliminate or reduce the effect of interferences due to mass overlap. In this type of instrument, both a magnetic sector and an electric sector are used to separate and focus the ions. The magnetic sector is dispersive with respect to both ion energy and mass and focuses all of the ions with diverging angles of motion that emerge from the entrance slit of the spectrometer. The electric sector is dispersive only to ion energy and focuses the ions onto the exit slit. This type of an arrangement is called a double-focusing high resolution mass spectrometer [3].

Recently, ICP-MS has become a favored technique for the fast and accurate determination of trace and ultratrace elements in many matrices due to its low sample consumption, high sensitivity, excellent precision, and potential for multi-element analysis [4]. However, isobaric and polyatomic interferences can significantly affect the accuracy of ICP-MS analyses, especially for radioisotopes. Suppression of these interferences has been the subject of many studies, which have been reviewed elsewhere [5]. The reduction of polyatomic interferences can be accomplished using direct (instrumental) and indirect (sample preparation and treatment) techniques. However, sector field ICP-MS (ICP-SFMS) cannot resolve all interference problems, especially when a resolution higher than 10000 is required to separate the analyte from the interference. This is the case for numerous interferences, such as  $^{87}\text{Rb}/^{87}\text{Sr}$ ,  $^{90}\text{Zr}/^{90}\text{Sr}$ , and  $^{137}\text{Ba}/^{137}\text{Cs}$ .

As an alternative to ICP-SFMS, quadruple ICP-MS with a collision/reaction cell (ICP-CRC-QMS) has been proposed as a method to reduce background noise and improve sensitivity for isotopic and trace analyses [6]. The collision-reaction cell has previously been used to eliminate one or more interfering species (isobaric or polyatomic) that limit the analysis of selected isotopes [7]. To accomplish this goal, a reacting gas injected into the cell must ideally react with the interfering species without further reaction with the analyte of interest [8]. This reacting gas can be selected on the basis of thermodynamic and kinetic data. Based on studies of ion kinetics, dynamics, and thermochemistry, gas-phase reaction chemistry can be used to overcome polyatomic interferences without significant reduction in sensitivity [9].

## 2. Interferences

The interferences that occur in inductively coupled plasma mass spectrometry can be divided into two sources, polyatomic ions and isobaric overlap. These interferences can significantly affect the determination of radioisotopes at trace and ultra-trace level.

### 2.1 Polyatomic ions

Polyatomic ions result from the short-lived combination of two or more atomic species, e.g.,  $\text{ArO}^+$ . Argon, hydrogen and oxygen are the dominate species present in the plasma, and these species may combine with each other or with elements from the analyte matrix. The major elements present in the solvents or acids used during sample preparation (e.g., N, S, and Cl) also participate in these reactions. The extent of polyatomic ion formation, and thus the effective interference problems, depend on many factors, including extraction geometry, operating parameters for the plasma and nebulizer systems and most importantly, on the sample matrix [10]. Most of the polyatomic ions can be resolved from the analyte by setting the mass spectrometer at high resolution. Figure 1 shows the spectrum at  $m/z = 56$  when 100 ppb of iron standard solution is aspirated. A gross peak was observed in low resolution mode ( $m/\Delta m = 300$ ), but the  $^{56}\text{Fe}$  isotope was resolved in high resolution mode ( $m/\Delta m = 5000$ ).

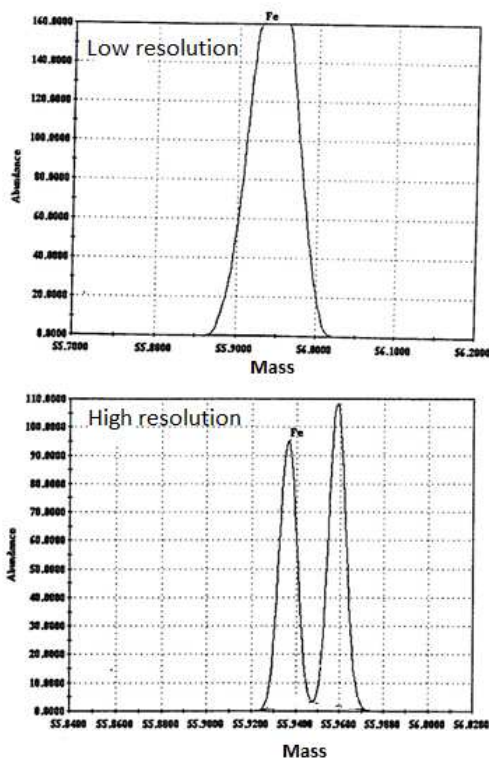


Figure 1. Mass spectra at  $m/z = 56$  measured for a 100 ppb iron standard solution at low and high resolutions.

## 2.2 Isobaric overlap

An isobaric overlap exists where two elements have isotopes of essentially the same mass that cannot be resolved by the conventional quadrupole or sector field mass analyzers [2]. Most of the elements in the periodic table have at least one (e.g., Co), two (e.g., Sm), or even three (e.g., Sn) isotopes that are free from isobaric overlap. No isobaric peak interference is observed for those isotopes below  $m/z = 36$ . For some elements, the most abundant, and therefore most sensitive isotope, may be subject to isobaric overlap, e.g.,  $^{48}\text{Ti}$  (73.7% abundant) and  $^{48}\text{Ca}$ . The severity of this type of interference is dependent to some extent on the sample matrix and relative proportions of the elements concerned. For example, Ba, La, and Ce all have an isotope at  $m/z = 138$ , and  $^{138}\text{Ba}$  is the most abundant isotope. If a sample needed to be analyzed for ultratrace levels of barium, then this isotope would be the preferred one because it provides the most sensitive measurement.

## 3. The collision/reaction cell

A collision/reaction cell consists of RF multipole ion guides enclosed in a cell that can be pressurized with a gas [11]. The reported length of the rods ranges from ~5 cm to 15 cm. Currently, four cell-based quadrupole instruments are commercially available. The Perkin Elmer SCIEX ELAN DRC utilizes a quadrupole ion guide. The Micromass Platform and Thermo Elemental PQ ExCell utilizes a hexapole ion guide. The Agilent 7500c, 7700, and 8800 utilize octopole ion guides. Octopole ion guides provide good ion transmission efficiency [8]. Quadrupoles are unique because they permit operation within a narrow bandwidth as well as operation in other modes that are highly selective with respect to the mass-to-charge ratio [9]. Another important aspect of RF multipole ion guides is the shape and depth of the confining potential well. The quadrupole has the steepest confining potential, i.e., the potential rises quickly from the center of the device to the rods, whereas hexapoles, octopoles, and higher order multipoles have progressively flatter potential well minima. These higher order multipoles thus provide higher ion transmittance as well as reduced scattering losses [11]. The wider potential well in an octopole allows the ions to occupy a larger volume, and the ions travel farther as they pass through the cell. A higher order multipole ion guide thus provides a greater gas thickness (at comparable pressures) when compared to a lower order multipole. Because the extent of reaction depends exponentially on the number of collisions, this increased thickness has an enormous effect on the extent of reaction and thus on the efficiency of the cell. Scattering losses are reduced in higher order multipoles [8]. Figure 2 shows a schematic of the cell-based quadrupole instruments.

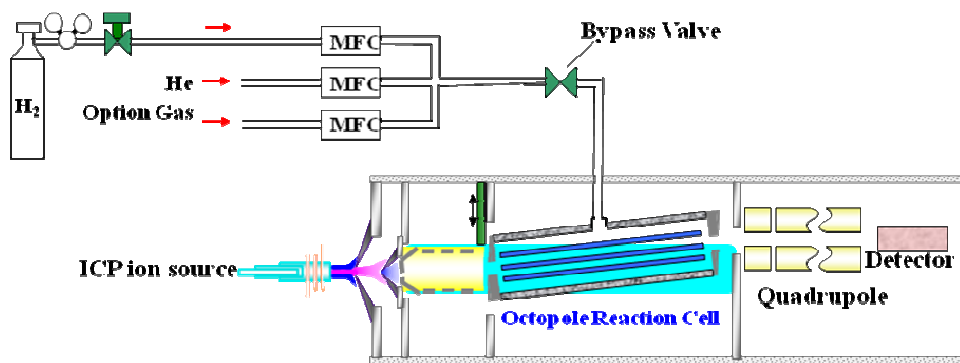


Figure 2. Schematic diagram of the single quadrupole mass spectrometer (Agilent 7500c).

Agilent Technologies has developed a new Triple Quadrupole mass spectrometer (ICP-QQQ) [12]. As shown in Figure 3, it has two quadrupoles, one before and one after the Collision/Reaction Cell. The first quadrupole selects ions to enter the cell, providing reliable reaction conditions to changing sample composition (MS/MS mode). It solves the problem of current cell technologies using reaction gas, allowing analysts to use reaction mode for more elements/isotopes applications, more effectively. Figure 2 and 3 illustrate the principle of two different models for ICP-MS. The comparison of the two modes is discussed in detail elsewhere [13-16]. In both cases, standard plasma conditions are employed.

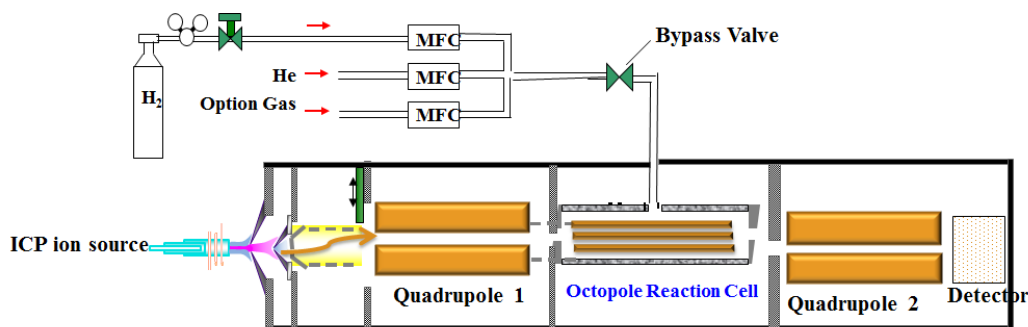


Fig. 3. Schematic diagram of the triple quadrupole mass spectrometer (Agilent ICP-QQQ 8800).

#### 4. Collisional processes

Ions entering the collision cell possess ion energy in a radial direction [17]. As ions enter the cell and collide with the inert gas atoms, energy transfer takes place, and the analyte ions lose energy. When the ions lose energy, the voltages applied to the reaction cell force the ions to move along the potential field, and the ions are subsequently confined within the potential region [18]. A small diameter cell (e.g., quadrupole) can be used to physically confine the ions into a tightly focused ion beam. This effect is known as collisional focusing and is required in systems having inherently low sensitivity or in which the reaction cell and the mass analyzer are of the same physical diameter. Collisional processes include energy transfer and collisional fragmentation.

##### 4.1 Energy transfer

In an elastic (no internal excitation), non-reactive collision of an ion of mass  $m_1$  and kinetic energy  $E_1$  with a stagnant ( $E_2 = 0$ ) neutral species of mass  $m_2$ , the energies after collision are given by Equations 1 and 2 [18].

$$\bar{E}_1 = E_1 \left[ \frac{m_1^2 + m_2^2}{(m_1 + m_2)^2} \right] \quad (1)$$

$$\bar{E}_2 = E_1 - \bar{E}_1 \quad (2)$$

As  $m_2 \rightarrow 0$ ,  $\bar{E}_1 \rightarrow E_1$  and no energy transfer occurs; the reactant ion departs the interaction with the same energy with which it entered. If  $m_2 = m_1$ , the collision partners exit with equal energy and the incident ion loses half of its initial energy. Multiple collisions of the ion result in sequential losses of kinetic energy and in energy damping, i.e.,

a reduction in the width and magnitude of the kinetic energy distribution. Thus, the ion loses energy according to the reduced mass of the collision partners, i.e., a larger neutral/ion mass ratio increases the rate of energy damping of the ion. Complete damping to the thermal condition, if possible, refers to an essentially 'random walk' executed by the ion through the cell [17]. A large ion energy at the entrance to the cell (source potential plus expansion energy minus cell offset potential) requires more collisions for energy damping. For a given cell pressure, a higher initial energy also results in a reduction in efficiency because the ion progresses farther into the cell before the energy is damped, and the number of collisions is consequently reduced. Furthermore, higher energy lowers the probability of reaction during a collision, compromises the specificity of the thermal chemistry, and increases the potential for sputtering cell materials.

#### 4.2 Collisional fragmentation

The transfer of energy to internal degrees of freedom during a collision defines an inelastic collision [19]. The energy that is transferred can be distributed amongst the various internal degrees of freedom; for a polyatomic ion, these include rotational, vibrational and electronic degrees of freedom. Subsequent collisions can transfer (relax) this energy to translation (kinetic energy, heat). If an energy that exceeds the bond strength accumulates in a single vibrational degree of freedom, the chemical bond may rupture, and the polyatomic ion fragments. Fragmentation may be successful in a single collision, in which case a relatively high collision energy is required to account for the distribution of the energy into the various degrees of freedom [20]. Fragmentation can also occur through multiple collisions, in which the internal energy is accumulated by sequential energy pumping to the dissociation limit.

#### 5. Kinetic energy discrimination using inert gas

Kinetic energy discrimination (KED) refers to the use of a potential barrier between the cell and mass analyzer, typically by operating the cell at a dc offset potential somewhat lower than that of the analyzing quadrupole. Beam ions from the ICP retain a significant portion of their original kinetic energy and trajectory, whereas ions formed inside the cell are typically formed at lower kinetic energy and/or off-axis trajectory [20]. The lower energy ions formed in the cell are unable to overcome the potential barrier and are thus prevented from passing into the analyzing quadrupole and on to the ion detector. In this approach, the low mass cut-off of the quadrupole is raised while the high mass stability edge is lowered. These conditions create a narrow window of masses that are stable in the quadrupole field [21]. For example, the monatomic ion ( $^{210}\text{Pb}$ ) and polyatomic ion ( $^{208}\text{Pb}^1\text{H}_2$ ) enter the cell with the same energy and collide with the inert gas (He), as shown in Figure 4. The molecular ion ( $^{208}\text{Pb}^1\text{H}_2$ ) has a larger cross section than the analyte at the same mass ( $^{210}\text{Pb}$ ) and experiences more frequent collisions with He; consequently,  $^{208}\text{Pb}^1\text{H}_2$  undergoes a significant reduction in kinetic energy relative to the analyte ( $^{210}\text{Pb}$ ). Energy filtering can be used to ensure only the analyte enters the quadrupole analyzer.

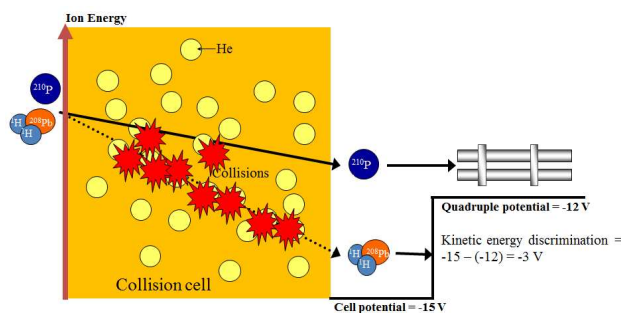
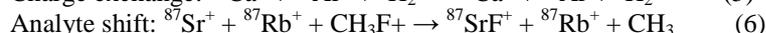
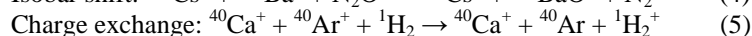
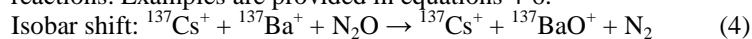


Figure 4. Energy discrimination between  $^{210}\text{Pb}$  and  $^{208}\text{Pb}^1\text{H}_2$  in the collision cell when He is used as the collision gas.

#### 6. Ion–molecule reaction chemistry

Although many different types of gas-phase, ion–molecule reactions exist, only a relative few have thus far been shown to play important roles in interferent reduction in ICP-MS [22,23]. Of course, thermodynamic and kinetic considerations must be considered when developing reaction chemistry strategies.. More fundamental aspects of ion thermochemistry can be found in Lias et al. [24]. Studies by Tanner and colleagues may be reviewed for a complete discussion of reaction thermodynamics and kinetics considerations in ICP-MS [25]. In brief, reactions must be thermodynamically allowed under the employed reaction conditions, i.e., they must be experimentally exothermic, and the reaction rates must be analytically useful. Compilations of thermodynamic data and reaction rates are available [25] and can/should be consulted as a guide for experiments, but empirical testing and verification under actual instrumental conditions is nonetheless advised.

To resolve two or more isobars, either the more intense isobar must be neutralized, or the interfering isobar or the analyte isobar must be shifted away from the other in terms of mass/charge. These conversions are accomplished using a variety of reaction types, including atom transfers, adduct formation, charge exchange, and condensation reactions. Examples are provided in equations 4-6.



Each of the above reactions resolves two isobars. However, these types of reactions can create other interfering ions. If other analyte isotopes are present at these mass/charge values, new interferences are potentially created. This consequence must be considered when designing reaction chemistry strategies and applications that use single quadrupole mass spectrometers.

The most useful reagent gases for ICP-MS can be classified as charge-exchange reagent gases (e.g., H<sub>2</sub>, NH<sub>3</sub>, Xe, CH<sub>4</sub>, and N<sub>2</sub>), oxidation gas reagents (e.g., O<sub>2</sub>, N<sub>2</sub>O, NO, and CO<sub>2</sub>), relatively few adduction gases (e.g., H<sub>2</sub> and CO), and other reagent gases (e.g., CH<sub>4</sub>, C<sub>2</sub>H<sub>6</sub>, C<sub>2</sub>H<sub>4</sub>, CH<sub>3</sub>F, SF<sub>6</sub>, and CH<sub>3</sub>OH). Gas ions with a low mass have the advantage of being converted to low m/z products, and they are easily swept or ejected from the reaction cell. In general, heavier gases are both more reactive, due to their higher cross-sections and better damping characteristics, and less specific [11]. The more appropriate reagent gases mostly react at high rates, are highly selective, and provide significant resolution efficiency from the interfering isobars. Therefore, the primary product ions are created rapidly and (preferably) completely. The secondary products are easily removed or minimally re-react, which results in minimal spectral complexities [11].

### 7. Applications of ICP-CRC-MS for the determination of Radioisotopes

Collision/reaction cell techniques are being applied to a continually increasing variety of sample types [26-93]. The applications cited here cover the 2000–2011 period (some early 2012 work is also referenced). This survey of applications constitutes an illustrative review and is not an exhaustive compilation. This fact is perhaps demonstrated by the increasing frequency with which ICP-CRC-MS elemental analyses are appearing in publications other than those of traditional elemental and atomic spectroscopy. Some of ion-molecule reactions and collisional fragmentations are discussed briefly below.

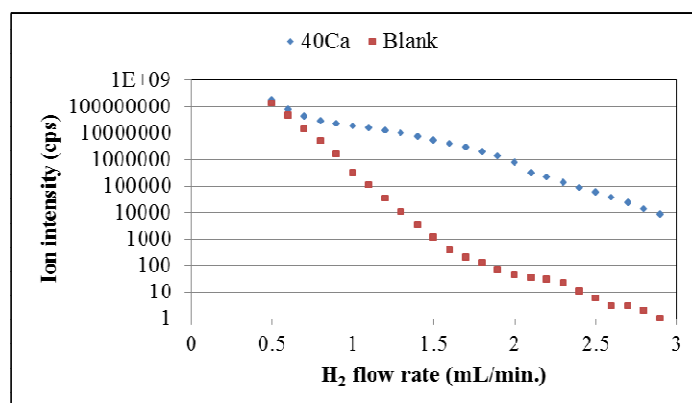


Figure 5. Separation of <sup>40</sup>Ar<sup>+</sup>/<sup>40</sup>Ca<sup>+</sup> with H<sub>2</sub> using ICP-CRC-MS.

#### 1.1 <sup>40</sup>K<sup>+</sup>/<sup>40</sup>Ar<sup>+</sup>/<sup>40</sup>Ca<sup>+</sup> and <sup>41</sup>Ca<sup>+</sup>/<sup>41</sup>K<sup>+</sup> separation with N<sub>2</sub>O

The N<sub>2</sub>O ionization potential is 12.886 eV, which makes charge-exchange reactions endothermic for most atomic cations [59]. The affinity of N<sub>2</sub> for an oxygen atom is relatively low (1.735 eV), which makes oxidation reactions exothermic for many cations. In some cases, nitration has been reported to compete with oxidation. Spin conservation may play a deciding role in exothermic oxidation reactions because the ground states of N<sub>2</sub>O and N<sub>2</sub> (the neutral product) are both singlets; thus, a reactant cation and a product oxide ion must have the same spin [18]. <sup>40</sup>Ar<sup>+</sup> and <sup>40</sup>Ca<sup>+</sup> interfere with the detection of <sup>40</sup>K<sup>+</sup> (T<sub>1/2</sub> = 1.28 × 10<sup>9</sup> a). The K<sup>+</sup>/Ar<sup>+</sup> ratio has been shown to be improved by nine orders of magnitude in reactions with ammonia or H<sub>2</sub>, however, Ca<sup>+</sup> is not suppressed as shown in Figures 5 and 6 [60]. K<sup>+</sup> is unreactive with N<sub>2</sub>O, but Ar<sup>+</sup> and Ca<sup>+</sup> are both reported to react with N<sub>2</sub>O [61]. Reaction profiles measured with ICP-DRC-MS show that K<sup>+</sup>/Ar<sup>+</sup> can be improved by more than three orders of magnitude, while K<sup>+</sup>/Ca<sup>+</sup> is enhanced by a factor of ~50 [62]. These improvement factors may be of interest for in situ analysis of interstellar grains. Recent super-nova material will be more enriched in <sup>40</sup>K than terrestrial material, so such an enhancement of K over Ca and Ar may be sufficient for analysis. The data also suggest that <sup>41</sup>Ca (T<sub>1/2</sub> = 1.03 × 10<sup>5</sup> a),

an important radionuclide used in dating and neutron flux monitoring [63], can be separated from  $^{41}\text{K}$  when it is measured as  $^{41}\text{CaO}^+$  at  $m/z = 57$ . Oxidation of  $\text{Ca}^+$  does not occur for every collision; however, about half of the ions are converted to the oxide, which should provide a significant improvement in  $\text{CaO}^+/\text{KO}^+$  as compared to  $\text{Ca}^+/\text{K}^+$ .

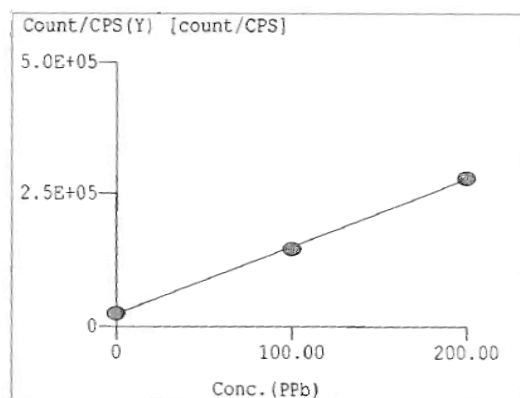


Figure 6. Calibration curve for  $^{40}\text{Ca}$  using  $\text{H}_2$  as the reactive gas in ICP-CRC-MS.

### 1.2 $^{59}\text{Ni}^+/\text{Co}^+$ separation with $\text{N}_2\text{O}$

$^{59}\text{Ni}$  ( $T_{1/2} = 7.6 \times 10^4$  a) and  $^{60}\text{Fe}$  ( $T_{1/2} = 1.5 \times 10^6$  a) are cosmogenic isotopes used in meteorite exposure dating.  $\text{Co}^+$  reacts with  $\text{N}_2\text{O}$  via oxidation and clustering faster than  $\text{Ni}^+$  and  $\text{Fe}^+$ , respectively [62]. Both cations exhibit exothermic oxidation reactions with  $\Delta H_r = -1.11$  and  $-0.37$  eV, respectively [62]. Bandura et al. [59] observed the formation of  $\text{NiO}^+$  and noticeable loss of  $\text{Ni}^+$ .

### 1.3 $^{60}\text{Fe}^+/\text{Ni}^+$ separation with $\text{N}_2\text{O}$

$\text{Fe}^+$  oxidation is faster than that of  $\text{Ni}^+$  and could theoretically be used for detection of  $^{60}\text{FeO}^+$ . Thus, there is no advantage in the detection of  $\text{Fe}^+$  as  $\text{FeO}^+$ . One possible detection method is to use  $\text{CH}_3\text{I}$ , which is reported to be reactive towards  $\text{Fe}^+$ , producing  $\text{FeI}^+$ , and less reactive towards  $\text{Ni}^+$  and  $\text{Co}^+$  [64].

### 1.4 $^{79}\text{Se}^+/\text{Br}^+$ separation with $\text{O}_2$

Selenium is one of the fission products which we find in irradiated fuels.  $^{79}\text{Se}$  is a long life fission product ( $T_{1/2} = 2.8 \times 10^5$  a), so it is of prime interest to determine precisely the quantity of  $^{79}\text{Se}$  produced during nuclear fuel irradiation. Indeed, this radio-isotope is one of the potential long term radio-contaminating elements, because of its capacity of migration in the various compartments of the ground [65,66]. The ionization potential of  $\text{O}_2$  is sufficiently high (12.07 eV) that exothermic oxidation channels are not possible for most cations. The O-atom affinity of O is 5.169 eV and provides the potential for good selectivity of oxidation reactions [67].  $^{79}\text{Br}$  interferes with the detection of  $^{79}\text{Se}$ .  $\text{Br}^+$  reacts slightly faster than  $\text{Ar}_2^+$  [68].  $\text{Se}^+$  is reported to form  $\text{SeO}^+$  when reacted with  $\text{O}_2$  in ICP-DRC-MS [59], and the reaction has been evaluated to be exothermic at  $-24$  kJ/mol (0.25 eV) [69]. Reactive loss of  $\text{Se}^+$  is not significant and is compensated for by collisional focusing. Brennetot, et al. [70] Optimized the operating conditions of a quadrupole ICP-MS with hexapole collision/reaction cell using a mixtures of gases ( $\text{O}_2$ ,  $\text{O}_2/\text{He}$ ,  $\text{O}_2/\text{Ne}$ ,  $\text{O}_2/\text{Ar}$  and  $\text{O}_2/\text{N}_2$ ) for the analysis of selenium-79 in spent nuclear fuel using experimental designs.

### 1.5 $^{90}\text{Sr}^+/\text{Zr}^+$ separation with $\text{O}_2$

Analysis of  $^{90}\text{Sr}$  is hampered by isobaric interferences from  $^{90}\text{Zr}$ - and Ar-based ionic species. The resolution of  $^{90}\text{Zr}$  from  $^{90}\text{Sr}$  requires a mass resolution of 98150, which is beyond the capability of ICP-SFMS. Previously published studies indicate that the reactive gases  $\text{CH}_3\text{F}$ ,  $\text{CH}_3\text{Cl}$ ,  $\text{SF}_6$ ,  $\text{NH}_3$ ,  $\text{D}_2\text{O}$ ,  $\text{CS}_2$ ,  $\text{CO}_2$ ,  $\text{N}_2\text{O}$ , and  $\text{O}_2$  could be used to remove isobaric and polyatomic interferences from Sr isotopes [71-76]. The heats of reaction of  $\text{O}_2$  with Sr, Zr, and Y ions were calculated to be 47.8 kcal/mol, -88.7 kcal/mol, and -60.4 kcal/mol, respectively [11]; these results indicate that the reaction with Sr is endothermic and not energetically favorable, whereas reactions with Zr and Y are exothermic and favorable. Tanner et al. [25] pointed out that kinetic data must also be considered to ensure that an exothermic reaction occurs in the reaction cell (because of the small contact time between gas molecules and ions). Data available from Koyanagi et al. [72] showed that the reactions of  $\text{O}_2$  with Zr and Y were efficient with yields of 82% and 67%, respectively, whereas no reaction between  $\text{Sr}^+$  and O was observed [73]. Figure 7 shows the reaction profiles for  $\text{Sr}^+$ ,  $\text{Zr}^+$  and  $\text{Y}^+$  ions with  $\text{O}_2$  that were measured using CRC-ICP-QMS. The concentrations of Sr, Zr and Y used for this investigation were 1 ppb. At flow rates below 1 mL/min, the  $^{89}\text{Y}^+$  and  $^{90}\text{Zr}^+$  signals decay relatively quickly, whereas the  $^{88}\text{Sr}^+$  signal increases up to a maximum flow rate of 1 mL  $\text{min}^{-1}$ .  $^{90}\text{Sr}$  detection was successful at 0.92 ppt with a 1-mL  $\text{min}^{-1}$   $\text{O}_2$  flow rate.

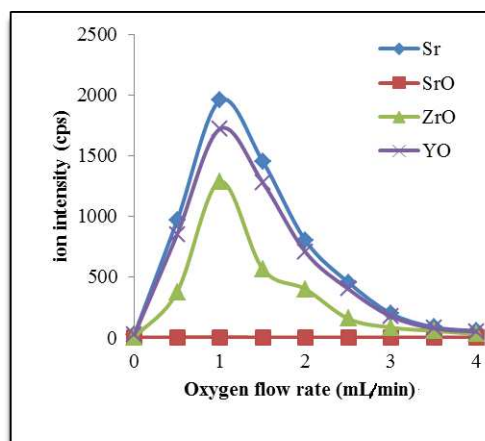


Figure 7. Effect of O<sub>2</sub> gas flow rate on the net signals of <sup>88</sup>Sr, <sup>89</sup>Y and <sup>90</sup>Zr. The Sr, Zr and Y concentrations were all 1 ppb.

### 1.6 <sup>93</sup>Mo/<sup>93</sup>Nb/<sup>93</sup>Zr separation with NO

<sup>93</sup>Mo ( $T_{1/2} = 3.5 \times 10^3$  a) may be useful in exposure dating and needs to be detected at ultra-low levels in nuclear waste [78]; <sup>93</sup>Mo can potentially be resolved from <sup>93</sup>Nb and <sup>93</sup>Zr ( $T_{1/2} = 1.5 \times 10^6$  a). Oxidation of Mo<sup>+</sup> by NO is endothermic at 1.61 eV and proceeds slowly via a two-step process, whereas oxidation of Nb<sup>+</sup> and Zr<sup>+</sup> is exothermic ( $\Delta H_f = -2.46$  and  $-2.48$  eV, respectively) [23,78].

### 1.7 <sup>129</sup>I/<sup>129</sup>Xe<sup>+</sup> separation with O<sub>2</sub>

The use of ICP-MS for determination of <sup>129</sup>I in environmental samples is complicated by interference from <sup>129</sup>Xe<sup>+</sup> originating from Xe present as an impurity in Ar plasma gas and by <sup>127</sup>IH<sub>2</sub><sup>+</sup> derived from <sup>127</sup>I in samples. Collision cell and reaction cell techniques have been used to reduce such interference [79,80]. Fujiwara et al. [81] used ICP-MS with the dynamic reaction cell (DRC) and axial field technology (AFT) to improve <sup>129</sup>I determination. The response characteristics of DRC-ICP-MS to test solutions with various <sup>129</sup>I and <sup>127</sup>I concentrations were investigated after instrument optimization. They eliminated <sup>129</sup>Xe<sup>+</sup> interference by using O<sub>2</sub> as the reaction gas, and effectively reduced <sup>127</sup>IH<sub>2</sub><sup>+</sup> interference by applying a negative AFT voltage and removing traces of H<sub>2</sub> and H<sub>2</sub>O from the reaction gas. Consequently, the background count ratio (mass 129/mass 127) decreased to the 10<sup>-8</sup> level. However, the relationship between the signal at mass 129 and <sup>129</sup>I concentration was nonlinear, and they attributed the nonlinearity to sensitivity degradation due to abundant <sup>127</sup>I in the matrix. They used a Rh internal standard for correcting the sensitivity degradation and obtained a linear relationship between mass 129/mass 103 and <sup>129</sup>I concentration. The detection limit for <sup>129</sup>I in a 1 mg mL<sup>-1</sup> <sup>127</sup>I matrix was 15.2 pg mL<sup>-1</sup>, which is equivalent to an <sup>129</sup>I/<sup>127</sup>I ratio of  $1.5 \times 10^{-8}$ . They used the developed method for the determination of <sup>129</sup>I in soil samples obtained from the land surrounding the nuclear fuel reprocessing plant in Tokai, Japan. The measured <sup>129</sup>I/<sup>127</sup>I ratios ( $2.6 \times 10^{-8}$  to  $4.7 \times 10^{-7}$ ) agreed with the ratios determined by tandemron accelerator mass spectrometry.

### 1.8 <sup>137</sup>La<sup>+</sup>/<sup>137</sup>Ba<sup>+</sup> and <sup>138</sup>La<sup>+</sup>/<sup>138</sup>Ba<sup>+</sup> separation with O<sub>2</sub>

The separation of <sup>138</sup>Ba<sup>+</sup> from <sup>138</sup>La<sup>+</sup> may be of interest for in situ studies of <sup>138</sup>Ba anomalies in early earth and meteorite samples. <sup>138</sup>La ( $T_{1/2} = 1.05 \times 10^{11}$  a) is used in <sup>138</sup>La–<sup>138</sup>Ce and <sup>138</sup>La–<sup>138</sup>Ba geochronometers. Detection of <sup>138</sup>La<sup>+</sup> is disrupted by highly abundant <sup>138</sup>Ba<sup>+</sup>. <sup>137</sup>La<sup>+</sup> ( $T_{1/2} = 6.0 \times 10^4$  a) is disrupted by <sup>137</sup>Ba<sup>+</sup>. Ba<sup>+</sup> oxidation by O<sub>2</sub> is endothermic by 1.15 eV and it is reported as non-reactive [82], and La<sup>+</sup> oxidizes at 0.75 eV [83]. ICP-DRC-MS reaction profiles show high reactivity of La<sup>+</sup>, but oxidation of up to 12% of Ba<sup>+</sup> is also observed at high O<sub>2</sub> flow [59]. The question of <sup>138</sup>Ce<sup>+</sup> separation from <sup>138</sup>La<sup>+</sup> arises when the chronometer is discussed. Ce<sup>+</sup> is oxidized by O<sub>2</sub> at a rate similar to La<sup>+</sup>, thus different chemistries have to be considered.

### 1.9 <sup>137</sup>Cs<sup>+</sup>/<sup>137</sup>Ba<sup>+</sup> and <sup>135</sup>Cs<sup>+</sup>/<sup>135</sup>Ba<sup>+</sup> separation with N<sub>2</sub>O

Three recent studies have illustrated that the Cs–Ba isobaric interference can be suppressed by H<sub>2</sub> and He mixtures, N<sub>2</sub>O, and CH<sub>3</sub>Cl [62]. However, H<sub>2</sub> and He efficiencies were found to require optimization after separation and preconcentration for Ba concentrations above 0.5 ppb [71].

The available thermodynamic data for N<sub>2</sub>O [84] indicate that only Ba should be reactive with this gas. The heat of the reaction of N<sub>2</sub>O with Cs<sup>+</sup> to form CsO<sup>+</sup> is endothermic at 106.3 kJ/mol, so the reaction is not likely to occur. However, the heat of the reaction of Ba<sup>+</sup> with N<sub>2</sub>O to form BaO<sup>+</sup> is exothermic and thermodynamically favorable at  $-236.8$  kJ/mol [22]. Because thermodynamic data only provide indications of the feasibility of the reactions, kinetic data must also be considered to investigate reaction efficiencies. A standard solution of 10 ppb Cs and 10 ppb Ba

was aspirated through an octopole reaction cell ICP-QMS [71]. The effects of N<sub>2</sub>O on the resulting ion intensities of Cs and Ba are shown in Figure 8. The <sup>133</sup>Cs signal increased for N<sub>2</sub>O flow rates up to 1.5 mL/min. No reaction products were observed for Cs with N<sub>2</sub>O in the cell. In contrast, the Ba signal, observed at mass 137, decreased rapidly and became negligible at a 1.5-mL/min N<sub>2</sub>O flow rate, and a maximum intensity was observed at mass 154, indicating the formation of <sup>138</sup>Ba<sup>16</sup>O. Additionally, a maximum intensity was reached at mass 155 for a higher gas flow rate (2 mL/min), which accounts for the asynchronous formation of <sup>138</sup>Ba<sup>16</sup>O<sup>1</sup>H as compared to BaO.

The reactions of Sb and Sn (100-ppb natural solutions) with N<sub>2</sub>O gas have also been investigated, and the formation of SbO and SnO species was observed with an oxide formation rate of about 0.1% for both elements at a N<sub>2</sub>O flow rate of 1.5 mL/min. Very low yields of SbO and SnO were expected because of the very low ionization rates of Sb and Sn at an RF power of 800 W (ionization energies of Sb and Sn are 8.641 eV and 7.344 eV, respectively) [22].

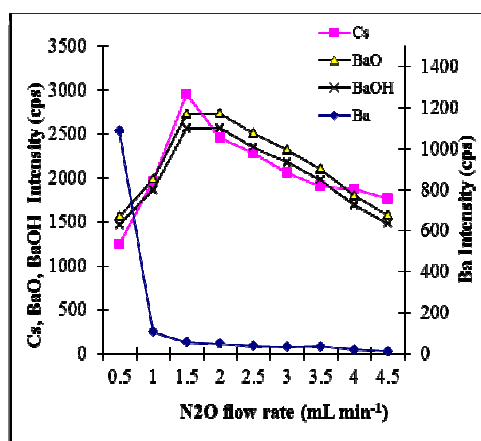


Figure 8. Effect of the N<sub>2</sub>O gas flow rate on the signal intensities of <sup>133</sup>Cs<sup>+</sup>, <sup>137</sup>Ba, <sup>138</sup>Ba<sup>16</sup>O, and <sup>138</sup>Ba<sup>16</sup>O<sup>1</sup>H at concentrations of 10 ppb Cs and 10 ppb Ba.

The fission product <sup>135</sup>Cs ( $T_{1/2} = 2.3 \times 10^6$  a) is an important isotope present in nuclear waste and fall-out and is also used as oceanic tracer. This isotope is also suggested for the <sup>135</sup>Cs–<sup>135</sup>Ba chronometer [86] and for improving the <sup>137</sup>Cs ( $T_{1/2} = 30$  a) chronometer [87].

#### 1.10 <sup>146</sup>Sm<sup>+</sup>/<sup>146</sup>Nd<sup>+</sup> separation with CO<sub>2</sub>

Oxidation of both Nd<sup>+</sup> and Sm<sup>+</sup> with CO<sub>2</sub> is exothermic ( $\Delta H_r = -2.35$  and  $-0.54$  eV, respectively) [70]. Relatively fast oxidation of Nd<sup>+</sup> was observed by Bandura et al. [59], and the Sm<sup>+</sup>/Nd<sup>+</sup> ratio was enhanced by a factor of more than 10<sup>4</sup> at flow of CO<sub>2</sub> = 1.4 mL/min [59]. The relatively low reactivity of Sm<sup>+</sup> limits its loss to a modest two fold [63].

#### 1.11 <sup>150</sup>Gd<sup>+</sup>/<sup>150</sup>Sm<sup>+</sup>/<sup>150</sup>Nd<sup>+</sup> separation with NO

<sup>150</sup>Gd<sup>+</sup> ( $T_{1/2} = 1.8 \times 10^6$  a) oxidation with NO is exothermic by 1.29 eV and has been shown to proceed at <1/2 of the capture rate [22], while its stable isobars <sup>150</sup>Sm<sup>+</sup> and <sup>150</sup>Nd<sup>+</sup> oxidize slowly. The product ion <sup>150</sup>GdO<sup>+</sup> can be detected at  $m/z = 166$  at relatively low flows of NO (before significant oxidation of Sm<sup>+</sup> and Nd<sup>+</sup> occurs), although presence of major isotope <sup>166</sup>Er may hinder detection because Er<sup>+</sup> is not oxidized with NO [59,22]. However, if mass selection is performed before the ion-molecule reactor, Er<sup>+</sup> spectral overlap will be absent.

#### 1.12 <sup>152</sup>Eu<sup>+</sup>/<sup>152</sup>Sm<sup>+</sup>/<sup>152</sup>Gd<sup>+</sup> separation with O<sub>2</sub>

Gueguen et al. [88] developed an analytical method by using a Multiple Collector-Inductively Coupled Plasma Mass Spectrometer (MC-ICP-MS, Isoprobe) equipped with a collision/reaction cell in order to circumvent the formation of isobaric interferences of Sm and Gd isotopes on Eu isotopes. They show that direct Eu isotopic ratios measurements are possible in the presence of O<sub>2</sub> used as reactant gas in the cell due to the opposite behaviour of Eu and Sm/Gd towards this gas. SmO<sup>+</sup> and GdO<sup>+</sup> oxide ions are fully formed whereas Eu is mainly present as Eu<sup>+</sup>. The separation efficiency of the Isoprobe's collision reaction-cell was studied on both natural Eu and certified <sup>153</sup>Eu enriched solutions. Accuracy of the measurement was found to be within the reference value uncertainty. Reproducibility of <sup>151</sup>Eu/<sup>153</sup>Eu isotopic ratio measurement were found to be lower than 0.3%, in the case of natural solution, and lower than 4‰ with the <sup>153</sup>Eu enriched solution, respectively. The study applied to measure the <sup>152</sup>Eu with high precision and accuracy.

**1.13  $^{176}\text{Lu}^+ / ^{176}\text{Hf}^+ / ^{176}\text{Yb}^+$  separation with NO**

The Lu-Hf dating method requires quantitation of Lu and Hf isotopes, including the overlapping  $^{176}\text{Lu}$  and  $^{176}\text{Hf}$  [89]. Because both isotopes are relatively abundant and the extent of separation does not need to be large, chemical resolution in a reaction cell may potentially be useful for in situ laser ablation analysis. Oxidation of  $\text{Hf}^+$  by NO is exothermic by 0.99 eV, whereas oxidation reactions of  $\text{Lu}^+$  and  $\text{Yb}^+$  are endothermic by 0.75 and 2.5 eV, respectively. Reaction profiles confirm that the oxidation of  $\text{Hf}^+$  is relatively fast [83], and  $\text{Lu}^+$  and  $\text{Yb}^+$  signals increase due to collisional focusing in the pressurized quadrupole [59].

**1.14  $^{187}\text{Re} / ^{187}\text{Os}$  separation with  $\text{N}_2\text{O}$** 

$^{187}\text{Re}$  ( $T_{1/2} = 4.35 \times 10^{10}$  a) is used in the  $^{187}\text{Re}$ - $^{187}\text{Os}$  geochronometer. Oxidation reactions of both  $\text{Re}^+$  and  $\text{Os}^+$  with  $\text{N}_2\text{O}$  are exothermic ( $\Delta H_r = -3.25$  eV and  $-2.6$  eV, respectively) [62]. The observed failure of  $\text{Re}^+$  to oxidize despite the significant exothermicity is attributed to the spin-forbidden transition between ground states of  $\text{Re}^+$  and  $\text{ReO}^+$  [62]. Reaction profiles measured with ICP-DRC-MS show that more than five orders of magnitude improvement for  $\text{Re}^+ / \text{Os}^+$  oxidation is achieved. The terminal product of  $\text{Os}^+$  oxidation appears to be  $\text{OsO}_4^+$ , so one could propose simultaneous detection of Re and Os based on  $\text{OsO}_4^+$ .

**1.15  $^{208}\text{Pb} / \text{H}_2$  removal from  $^{210}\text{Pb}$  using Kr**

$^{210}\text{Pb}$  is found in the environment at activities ranging from a few millibecquerels to several becquerels, depending on the studied medium. These activities, converted to masses, represent only a few femtograms of this isotope and are significantly lower than the typical detection limits of most ICP-MSs using direct aspiration nebulization. Thus, pre-concentration of the sample is likely necessary to increase the number of atoms detected [24].

Although there is no stable isotope with a mass of 210, two of the short-lived radioactive daughters of  $^{210}\text{Pb}$  ( $^{210}\text{Bi}$  and  $^{210}\text{Po}$ ) have similar masses, so these isotopes may potentially interfere with the measurement of radio-lead at  $m/z = 210$ . Investigations of the background at  $m/z = 210$  with spiked solutions have shown that the concentration of stable Pb affects the  $^{210}\text{Pb}$  signal. The background count was about  $70 \pm 13$  cps when the stable Pb concentration was 100 ppb. Epov et al. [90] observed 9-100 cps at  $m/z = 210$  for a solution composed of only 2%  $\text{HNO}_3$ . Dissociation of some weak polyatomic ions formed from the NORM matrix due to the addition of unreactive krypton gas into the collision cell was studied. Collision cells aid the removal of polyatomic interferences through a combination of collisional interactions and energy discrimination [25]. Efficiency in collision mode is greatly improved by a shield torch system, which produces ions with very low and uniform ion energies. Polyatomic ions, which are larger than monatomic analyte ions, undergo more collisions with the Kr cell gas and lose more energy. Kr was chosen in this experiment because the radius of a Kr atom is larger than that of a He atom. Pressurizing the collision cell with Kr gas results in its collision with interfering polyatomic ions and the analyte ions. Because collisions with the polyatomic ions occur more frequently than those with the analyte ions due to their size, there is a selective decrease in polyatomic ion energy (Figure 9). The application of an energy difference potential between the octopole (-15 V) and quadrupole (-12 V) stops the lower energy polyatomic ions from entering the quadrupole while allowing the passage of the analyte ions under investigation. Kr was used as the collision cell gas at a flow rate of 0.4 mL/min throughout the experiments to minimize interferences, as demonstrated by the improvement in the isotope ratio of lead ( $^{208}\text{Pb} / ^{206}\text{Pb}$ ) as the Kr flow rate was changed from 0 to 0.8 mL/min (Figure 9). The detection limit was calculated from the calibration curve using standard solutions of  $^{210}\text{Pb}$  (5, 10, and 50 ppt). The detection limit for  $^{210}\text{Pb}$  was 0.214 ppt (0.604 Bq/mL) [23].

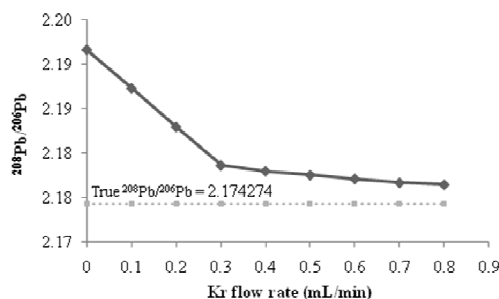


Figure 9. Improvement in the isotope ratio  $^{208}\text{Pb} / ^{206}\text{Pb}$  as the Kr gas flow rate increases.

**1.16  $^{238}\text{U} / ^{238}\text{Pu}$  separation with  $\text{CO}_2$** 

One of the major hindrances to analyzing Pu isotopes using ICP-MS is the occurrence of the  $^{238}\text{U}$ - $^{238}\text{Pu}$  isobaric and  $\text{UH}^+$  ion as  $^{239}\text{Pu}$  interferences. Santos et al. [91] examined the oxidation of  $\text{Th}^+$ ,  $\text{U}^+$ ,  $\text{Np}^+$  and  $\text{Pu}^+$  with  $\text{N}_2\text{O}$ ,  $\text{C}_2\text{H}_4\text{O}$ ,  $\text{H}_2\text{O}$ ,  $\text{O}_2$ ,  $\text{CO}_2$ ,  $\text{NO}$  and  $\text{CH}_2\text{O}$ . All of the actinide (An) ions formed corresponding  $\text{AnO}^+$  species with the exception

of  $\text{Pu}^+$ , which did not react with  $\text{CH}_2\text{O}$ . Vais et al. [92] evaluated the reaction of  $\text{O}_2$  and  $\text{NH}_3$  with U and Pu in the bandpass reaction cell or dynamic reaction cell (DRC) of the ELAN DRC II mass spectrometer. Both U and Pu demonstrated similar reactivity with  $\text{O}_2$ , giving rise to the corresponding oxides. However, remarkable selectivity in their reaction with  $\text{NH}_3$  was observed. While U was rapidly converted into  $\text{UNH}_2^+$  and  $\text{UN}_2\text{H}_4^+$ , Pu remained unreactive in the DRC pressurized with  $\text{NH}_3$ . This difference in reactivity enabled the determination of Pu isotopes in urine and water samples containing excess U without a preceding separation procedure. Gourgiotis et al. [93] separated Pu from U by adding  $\text{CO}_2$  as a reactive gas to the collision-reaction cell of the ICP-MS. Vais et al. [92] demonstrated that the different reactivities of Pu and U toward  $\text{CO}_2$  gas permit the accurate and precise measurement of Pu and U isotopes in their  $\text{Pu}^+$  and  $\text{UO}_2^+$  forms with two different  $\text{CO}_2$  gas flow rates:  $0.4 \text{ mL min}^{-1}$  for  $\text{Pu}^+$  and  $1.5 \text{ mL min}^{-1}$  for  $\text{UO}_2^+$ .

## CONCLUSION

In just a few short years, collision/reaction cell techniques have been developed to the point where they offer unique interference reduction potential for ICP-MS analysis. Complex spectral interferences can be minimized or avoided completely using low-cost instrumentation and readily available gaseous reagents. The required ion-molecule chemistry knowledge is largely available through years of fundamental studies reported in the literature, and there is significant potential for new advances and improvements in the application of these techniques for radioisotopes determination at ultra-trace level.

With better performance than conventional reaction cell ICP-MS, ICP-MS-CRC-MS configuration will offer unrivaled flexibility for solving difficult applications, and new opportunities for advanced research. This configuration will be providing precise control of reaction processes in the collision/reaction cell. This ensures reaction mode results are consistent and reliable, even when the sample composition is complex or variable. For example, if mass selection is performed by the first MS before the ion-molecule reactor, the product ion  $^{150}\text{Gd}^{16}\text{O}^+$  can be detected at  $m/z$  166 with absence of  $^{166}\text{Er}$ . Another example is detection of  $^{40}\text{Ca}^{16}\text{O}$  and  $^{41}\text{Ca}^{16}\text{O}$  with absence of  $^{56}\text{Fe}$  and  $^{57}\text{Fe}$ .

## Acknowledgements

This article was made possible by a NPRP award [NPRP4-1105-1-173] from the Qatar National Research Fund (a member of The Qatar Foundation).

## REFERENCES

- [1] Balcaen L, Moens L, Vanhaecke F, *Spectrochim. Acta*, **2010**, 65B, 769.
- [2] Baba AA, Adekola FA, Olumodeji OO, Lawal M, *Advances in Applied Science Research*, **2011**, 2, 117.
- [3] Kutchera W, *Int J Mass Spectrom*, **2005**, 242, 145.
- [4] Helal AL, Zahran NF, Amr MA, Abdel El-Lateef AM, Baster II, Mohsen HT, Abbas Y, *Radiochem Acta*, **2004**, 92, 369.
- [5] Hou X, Roos P, *Anal Chim Acta*, **2008**, 608, 105.
- [6] Becker JS, Sela H, Dobrowolska J, Zoriy M, Becker JSU, *Int. J. Mass Spectrom*, **2008**, 270, 1.
- [7] Duzgoren-Aydin NS, Avula B, Willett KL, Khan IA, *Environ. Monit Assess*, **2011**, 127, 51.
- [8] Tonietto GB, Godoy JM, Oliveira A.C, De Souza MV, *Anal Bioanal Chem.*, **2010**, 397, 1755.
- [9] Alsenz H, Zereini F, Wiseman CLS and Püttmann W, *Bioanal Chem*, **2009**, 395, 1919.
- [10] Vonderheide AP, Zoriy MV, Izmer AV, Pickhardt C, Caruso JA, Ostapczuk P, Hille R., Becker JS, *J Anal At Spectrom*, **2004**, 19, 675.
- [11] Koppelaar DW, Eiden GC, Barinaga CJ, *J Anal At Spectrom*, **2004**, 19, 561.
- [12] Mizobuchi K, Sugiyama N, *Winter Plasma Conference on Plasma Spectrochemistry for Trace Element, Stable Isotope, and Elemental Speciation Analyses, Tucson, Arizona, USA, January 9 – 14, 2012*, Agilent publication, 5990-9755EN.
- [13] Kuwabara T, Yamada N, Kitamoto J, Yamada H, Kondo T, *Winter Plasma Conference on Plasma Spectrochemistry for Trace Element, Stable Isotope, and Elemental Speciation Analyses, Tucson, Arizona, USA, January 9 – 14, 2012*, Agilent publication, 5990-9755EN.
- [14] Takakashi J, Yamada N, *Winter Plasma Conference on Plasma Spectrochemistry for Trace Element, Stable Isotope, and Elemental Speciation Analyses, Tucson, Arizona, USA, January 9 – 14, 2012*, Agilent publication, 5990-9755EN.
- [15] Shikamori Y, Nakano K, Sugiyama N, Kakuta S, *Winter Plasma Conference on Plasma Spectrochemistry for Trace Element, Stable Isotope, and Elemental Speciation Analyses, Tucson, Arizona, USA, January 9 – 14, 2012*, Agilent publication, 5990-9755EN.

- [16] Sugiyama N, *Reaction Cell Frontier: Winter Plasma Conference on Plasma Spectrochemistry for Trace Element, Stable Isotope, and Elemental Speciation Analyses, Tucson, Arizona, USA, January 9 – 14, 2012*, Agilent publication, 5990-9755EN.
- [17] Isnard H, Aubert M, Blanchet P, Brennetot R, Chartier F, Geertsen V, Manuguerra F, *Spectrochim Acta*, , **2006**, 61B ,150.
- [18] Tanner SD, Baranov VI, Bandura DR, *Spectrochim Acta*, **2002**, 57B, 1361.
- [19] Simpson LA, Hearn R, Merson S, Catterick T, *Talanta*, **2005**, 65, 900.
- [20] Cheng P, Koyanagi G.K, Bohme DK, *Anal. Chim. Acta*, **2008**, 627,148.
- [21] Darrouzès J, Bueno M, Lespès G, Holeman M, Potin-Gautier M, *Talanta*., **2007**, 71, 2080.
- [22] <http://www.chem.yorku.ca/profs/bohme/research/research.html>.
- [23] Amr M.A, Al-Saad K.A, Helal AI, *Nucl. Instrum. Meth. A.*, **2010**, 615, 237.
- [24] Lias S.G, Bartmess J.E, Liebman J.F, Holmes J.L, Levin R.D, Mallard WG, *J Phys Chem Ref* , **1988**, 17, 1 (also see <http://webbook.nist.gov/chemistry/>).
- [25] Tanner SD, Baranov VI, Vollkopf U, *J Anal Atom Spectrom*, **2000**, 15, 1261.
- [26] Xiaole Sun, Per Andersson, Magnus Land, *J Anal At Spectrom*, **2010**, 25, 156.
- [27] Olesik JW, Jones DR, *J Anal At Spectrom*, **2006**, 21, 141.
- [28] Guoa W, Hua S, Lib X, Zhaob J, Jinb S, Liub W, Zhang H, *Talanta*, **2011**, 84, 887.
- [29] Tanner SD, Li CS, Vais V, Baranov VI, Bandura DR, *Anal. Chem.*, **2004**, 76, 3042.
- [30] Taylor VF, Jackson BP, Chen CY, *Bioanal Chem*, **2008** ,392,1283.
- [31] Gonzales E. R, Garcia S. R, Mahan C, Hang W, *J Radioanal Nucl Chem*, **2005**, 263, 457.
- [32] Baranov VI, Bandura DR, Tanner SD, *Int J Mass Spectrom*, **2005**, 247, 40.
- [33] Litherland AE, Tomski I, Doupe JD, *Nucl Instrum. Meth. B*, **2003**, 204, 720.
- [34] Caraiman D, Koyanagi GK, Bohme DK, *J Phys Chem A*, **2004**, 108, 978.
- [35] Vonderheide AP, Meija J, Tepperman K, Puga A, Pinhas A. R, States JC, Caruso JA, *J Chromatog A*, **2004**, 1024, 129.
- [36] Huerta VD, Reyes LH, Marchante-Gayon JM, Sanchez MLF and Sanz-Medel A, *J Anal At Spectrom*, **2003**, 18, 1243.
- [37] Bandura DR, Ornatsky OI, Liao L, *J Anal At Spectrom*, **2004**, 19, 96.
- [38] Chrastrný V, Komárek M, *Chem Pap*, **2009**, 63, 512.
- [39] Chrastrný V, Komárek M, Mihaljevič M, Štichová J, *Anal Bioanal Chem*, **2006**, 385, 962.
- [40] Doupe JP, Litherland AE, Tomski I, Zhao XL, *Nucl Instrum Meth B*, **2004**, 223, 323.
- [41] Alsenz H, Zereini F, Wiseman CLS, Püttmann W, *Environ Sc Eng, Urban Airborne Particulate Matter*, **2011**, 261, 1.
- [42] Guo Y, Michael Siu KW, Baranov VI, *J Am Soc Mass Spectr*, **2005**, 16, 957.
- [43] Sun Q, Yuan D, Chen Z, Megharaj M, Naidu R, *Microchim Acta*, **2010**, 169, 41.
- [44] Popp M, Hann S, Mentler A, Fuerhacker M, Stingeder G, Koellensperger G, *Anal Bioanal Chem*, **2008**, 391, 695.
- [45] Favre G, Brennetot R, Chartier F, Vitorge P, *Int J Mass Spectrom*, **2007**, 265, 15.
- [46] Suresh K, Danadurai K, Chellam S, Lee CT, Fraser MP, *Anal Chim Acta*, **2011**, 686, 40.
- [47] Arnold T, Harvey JN, Weiss DJ, *Spectrochim Acta B*, **2008**, 63, 666.
- [48] Avula B, Wang Y-H, Duzgoren-Aydina NS, Khan IA, *Food Chem*, **2011**, 127, 54.
- [49] Baker JA, Schiller M, Bizzarro M, *Geochim Cosmochim Ac*, **2012**, 77, 415.
- [50] Isnard H, Moureau J, Quidelleur S, Gueguen F, Granet M, Favre G, Nonell A, Chartier F, *proceeding of Advancements in Nuclear Instrumentation Measurement Methods and their Applications conference (ANIMMA), Marseille, France, 7-10 June 2009*, 1.
- [51] Nriagu J, Nam DH, Ayanwola TA, Dinh H, Erdenechimeg E, Ochir C, Bolormaa TA, *Sci. Total Environ.*, **2012**, 414, 722.
- [52] Boulyga SF, *Int. J. Mass Spectrom.*, **2011**, 307, 200.
- [53] Vajda N, Kim CK, *Appl. Radiat. Isotopes*, **2010**, 68, 2306.
- [54] Matthews DL, Leybourne MI, Peter JM, Scott SD, *J Anal At Spectrom*, **2006**, 21, 41.
- [55] Abbas K, Cydzik I, Torchio RD, Farina M, Forti E, *J Nanopart Res*, **2010**,12, 2435.
- [56] Carter S, Fisher AS, Goodall PS, Hinds MW, Lancastere S, Shore S, *J Anal At Spectrom*, **2011**, 26, 2319.
- [57] Butler OT, Cairns W, Cook JM, Davidson CM, *J Anal At Spectrom*, **2011**, 26, 250.
- [58] Kadar A, Noël L, Chekri R, Vastel C, Millour S, Guérin T, *Talanta*, **2011**, 85, 2605.
- [59] Bandura D.R, Baranov VI, Litherland AE, Tanner SD, *Int J Mass Spectrom*, **2006**, 256, 312.
- [60] Jung K, Yoshida T, Hasegawa S, *J Anal At Spectrom*, **2012**, 27, 131.
- [61] Marshall AG, Hendrickson CL, *Int J Mass Spectrom*, **2002**, 215, 59.
- [62] Lavrov VV, Blagojevic V, Koyanagi GK, Orlova G, Bohme DK, *J Phys Chem A*, **2004**, 108, 5610.
- [63] Martin C, Duchene S, Luis B, Goncalves P, Deloule E, Fournier C, *Mineral Petrol.*, **2010**, 159 , 437.
- [64] Pick D, Leiterer M, Einax JW, *Microchem J*, **2010** ,95 ,315.

- [65] Al-Saad KA, Amr MA, Helal AI, *Biol Trace Elem Res*, **2011**, 14, 103.
- [66] Elwaer N, Hintelmann H, *Talanta*, **2008**, 75, 205.
- [67] Bandura DR, Baranov VI, Tanner SD, *J Am Soc Mass Spectrom*, **2002**, 13 1176.
- [68] Hattendorf B, Günter D, *Spectrochim. Acta.*, **2003**, 58B, 1.
- [69] Anicich VG, *J Suppl Ser*, **1993**, 84, 215. (also available from <http://techreports.jpl.nasa.gov/2003/03-2964.pdf>).
- [70] Brennetot R, Pierry L, Atamyan T, Favre G, Vailhen D, *J Anal At Spectrom*, **2008**, 23 , 1350.
- [71] Amr MA, Abdel-Lateef AM, *Int J Mass Spectrom*, **2011**, 299, 184.
- [72] Koyanagi GK, Zhao X, Blagojevic V, Jarvis MJY, *Int J Mass Spectrom*, **2005**, 241 , 189.
- [73] Nadeau MJ, Lee HW, Litherland AE, Purser KH, Zhao XL, *Nucl Instrum Meth B*, **2004**, 223, 328.
- [74] Feuerstein J, Boulyga SF, Galler P, Stingeder G, Prohaska T, *J Environ Radioactiv*, **2008**, 99, 1764.
- [75] Kroening KK, Richardson DD, Afton S, Caruso JA, *Anal Bioanal Chem*, **2009**, 393, 1949.
- [76] Flores CR, Figueroa JAL, Wrobel K, Wrobel K, *Eur Food Res Technol*, **2009**, 228, 951.
- [77] Artigalás H, Debrun JL, Kilius L, Zhao XL, Litherland AE, Pinault JL, Fouillac C, Maggioro CJ, *Nucl Instrum Meth B*, **1994**, 92, 227.
- [78] Blagojevic V, Flaim E, Jarvis MJY, Koyanagi GK, Bohme DK, *J Phys Chem A*, **2005**, 109, 11224.
- [79] Johnson L, Günther-Leopold I, Kobler Waldis J, Linder HP, Low J, Cui D, Ekeröth E, Spahiu K, Evins L.Z, *J Nucl Mater*, **2012**, 420 , 54.
- [80] Nakano K, Shikamori Y, Sugiyama N, Kakuta S, *Winter Plasma Conference, Zaragoza, Spain, Jan 30th–Feb 4th 2011. Agilent publication, 5990-8171EN*, February **2011**, available from [www.agilent.com/chem/icpms](http://www.agilent.com/chem/icpms).
- [81] Fujiwara H, Kawabata K, Suzuki J, Shikino O, *J Anal. A. Spectrom*, **2011**, 26, 2528.
- [82] Lopatin SI, Shugurov S M, Stolyarova VL, Turnina ZG, *J. Chem. Thermodyn.*, **2006**, 38,1706.
- [83] Koyanagi GK, Bohme D, *J Phys Chem A*, **2001**, 105, 8964.
- [84] Granet M, Nonell A, Favre G, Chartier F, Isnard H, Moureau J, Caussignac C, *Spectrochim Acta B*, **2008**, 63, 1309.
- [85] Sun Q, Yuan D, Chen Z, Megharaj M and Naidu R, *Microchim Acta*, **2010**, 169, 41.
- [86] Hidaka H, Ohta Y, Yoneda S, DeLaeter JR, *Earth Planet Sc. Lett*, **2001**, 193, 459.
- [87] Taylor V F, Evans R D, Cornett RJ, *J Environ. Radioac*, **2008**, 99, 109.
- [88] Gueguen F, Nonell A, Granet M, Favre G, Isnard H, Chartier F, *J Anal At Spectrom*, **2010**, 25, 201.
- [89] Blichert-Toft J, Boyet M, Télouk P, Albarède F, *Earth Planet Sc Lett*, **2002**, 204, 167.
- [90] Epov VN, Taylor V, Lariviere D, Evans R.D, Cornett RJ, *J Radioanal Nucl Chem*, **2003**, 258, 473.
- [91] Santos M, Marcalo J, Pires de Matos A, Gibson J.K, Haire RG, *J Phys Chem A*, **2002**, 106, 7190.
- [92] Vais V, Li C, Cornett J, *Anal Bioanal Chem*, **2004**, 380, 235.
- [93] Gourgiotis A, Granet M, Isnard H, Nonell A, Gautier C, Stadelmann G, Aubert M, Durand D, Legand S and Chartier F, *J Anal At Spectrom*, **2010**, 25, 1939.